TOWARDS A 100mA SUPERCONDUCTING RF PHOTOINJECTOR FOR B*ERL*inPro *

A. Neumann†, W. Anders, A. Burrill, A. Jankowiak, T. Kamps, J. Knobloch, O. Kugeler, P. Lauinger, A. N. Matveenko, M. Schmeißer, J. Voelker (HZB, Berlin),
S. Schubert, J. Smedley (BNL, Upton, Long Island, New York),
J. Sekutowicz (DESY, Hamburg)
E. Zaplatin (FZJ, Julich)¨
V. Volkov (BINP SB RAS, Novosibirsk),
G. Ciovati, P. Kneisel (JLAB, Newport News, Virginia)
I. Will (MBI, Berlin)
R. Nietubyc (NCBJ, Swierk/Otwock)

Abstract

For BERLinPro, a 100 mA CW-driven SRF energy recovery linac (ERL) demonstrator facility, HZB needs to develop a photo-injector superconducting cavity which delivers a at least 1mm·mr emittance beam at high average current. To address these challenges of producing a high peak brightness beam at high repetition rate, at first HZB tested a fully superconducting injector with a lead cathode [1, 2], followed now by the design of a SC cavity for operation up to 4 mA. It uses CW-modified TTF-III couplers and a normal conducting high quantum efficiency (QE) cathode using the HZDR-style insert scheme. This talk will present the latest results and an overview of the measurements with the lead cathode cavity, we also describe the design and optimization process, the first production results of the current design and an outlook to the further development steps towards the full power version.

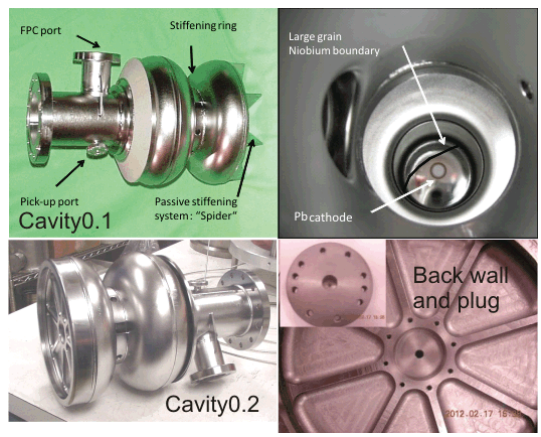

Figure 1: Pictures of cavity 0.1 with lead cathode plasma arc deposited on the back wall (top row) and cavity 0.2 with a lead coated plug version simplifying the deposition.

INTRODUCTION

For B*ERL*inPro HZB needs to develop a SRF photoinjector cavity which has to fulfill demanding requirements with respect to beam properties and SRF systems. B*ERL*inPro is a high current 100 mA 50 MeV energy recovery linac aiming to combine high peak brightness, small emittance and short pulse electron bunches with an average current comparable with the storage ring regime of hundreds of mA [3].

Therefore the injector cavity has to produce a small emittance beam at high peak brightness, which demands a high QE cathode with prompt response time and a low work function for operation with state of the art laser systems at high repetition rate. Further the cavity needs to handle beam power of 230 kW to accelerate the 100 mA beam to at least 2 MeV kinetic energy. To compensate for space charge driven beam expansion, the emission process has to take place at field levels as high as possible. The latter requirement as well as the low work function is competing with the demand, that the level of dark current needs to be omitted to a level as low as possible. This is mandatory to avoid beam halo formation and loss in the ERL, especially within the recirculator.

To account for all these diverging challenges, HZB has started an injector cavity test programm in collaboration with JLab, DESY, NCBJ, BNL, BINP, FZJ, HZDR and MBI in a three stage approach. The first step was to test and understand the beam dynamics of a one and a half cell injector cavity, which is an interesting candidate for CW driven low average current free electron lasers, a hybrid lead cathode niobum 1.6 cell injector cavity designed by J. Sekutowicz [4]. Here, the experimental results of two versions of this cavity which have been tested between 2011 and 2012 will be described.

The following step is a cavity with a new RF design [5] allowing for improved beam dynamics properties [6] and a high brightness beam introducing a normal conducting high QE cathode into the SC cavity using the HZDR style choke cell and insert system [7]. This cavity is currently being manufactured at JLab and awaiting the welding of the half cells and first processing and vertical testing. The

* Work supported by Bundesministerium für Bildung und Forschung and EuCARD SRF
† Axel.Neumann@helmholtz-berlin.de

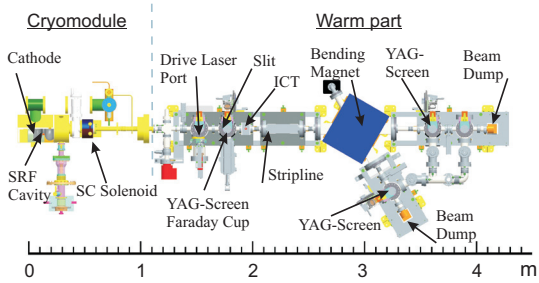

Figure 2: Experimental set up of the cavity measurement at the HoBiCaT horizontal test facility including cold section and warm diagnostic beam line for beam visualization as well as energy and current measurements.

design will be presented in the second half of this paper.

The third step will be a high power modification of the current design using two modified KEK-style [8] fundamental power couplers and being more optimized with respect to HOM properties and propagation.

HYBRID LEAD NIOBIUM CAVITY

Two versions of the hybrid PbNb cavity (see Figure 1) have been fabricated at JLab and received the superconducting lead cathode at NCBJ in Swierk(Poland) [9]. After completion of the cavity production and cathode deposition by plasma arc discharge, the cavity received its ancillary components and was installed within the HoBiCaT horizontal test facility at HZB, which was extended with a diagnostic beam line. This setup is shown in Figure 2.

For the first cavity the lead spot was deposited on the back wall by mounting the whole structure to the deposition system. Afterwards the cavity received a final short BCP and HPR using a protective mask for the cathode in order to remove remnants by the plasma arc process [10]. This cavity was operated without any tuner and thus received a strong back wall stiffening. It was equipped with an adjustable TTF-III coupler, allowing external Qs ranging from $1 \cdot 10^9$ down to $6 \cdot 10^6$ including a three-stub tuner [11]. The second cavity features an improved back wall stiffening, molding the stiffener bars directly out of the back wall material, a modified Saclay-I style tuner system and a niobium plug in the center of the back wall. The plug system allowed for a more direct and uniform formation of the cathode as it was installed very close to the lead source of the deposition set up. Improvements and obstacles due to this construction will be discussed in the following sections. Table 1 summarizes the simulated and measured RF properties of both cavities. Note, that significant higher field levels and thus beam energies were achieved with the plug cavity.

Quality Factor

Given in Figures 3, 4 and 5 are the unloaded quality factors Q_0 as a function of the peak on axis field E_0, located at the cathode, as measured after the final assembly in the vertical test stand with and without lead cathode compared to the values achieved within the horizontal beam production set up. Note, that the vertical tests were done at 2.0 K, while the horizontal ones at 1.8 K. The bare cavities achieved low field Q_0s of the order of $2{\cdot}10^{10}$ reaching maximum fields up to a quench field of 45 MV/m for cavity 0.1 and 55 MV/m for cavity 0.2. It is in common for the back wall and plug set up, that both cavities saw an increase by a factor of two of the surface resistance after receiving the lead cathodes. This seems to be a general contamination problem rather than additional dissipation in the lead film, as can be seen by RF calculations (see Figure 6), that the peak magnetic field is only 2 mT at 20 MV/m. The fraction of the cathode losses to the total cavity losses as-

Table 1: Cavity figures of merit for the TM_{010}-π mode of the hybrid lead cathode niobium 1.6 cell cavity for E_0= 27 MV/m. Note, that all parameters except the first four RF properties are measured values. The latter were obtained by Superfish and CST MWS simulations.

Parameter	Cavity 0.1&0.2
$R/Q(\Omega)$	190
E_{peak}/E_0	1.2
$E_{cathode}/E_0$	1.0
B_{peak}/E_{peak} (mT/(MV/m))	4.4
$\Phi_{launch}(E_{kin,max})$ (deg.)	15
E_{launch} (MV/m)	5&7
E_{kin} (MeV)	1.8&2.5
k_{cc} (%)	1.47
Q_{ext}	$6.6 \cdot 10^6$
$f_{1/2}$(Hz)	98
$P_{forward}$ (kW)	≤ 2
Δf_{peak} (Hz)	20-40

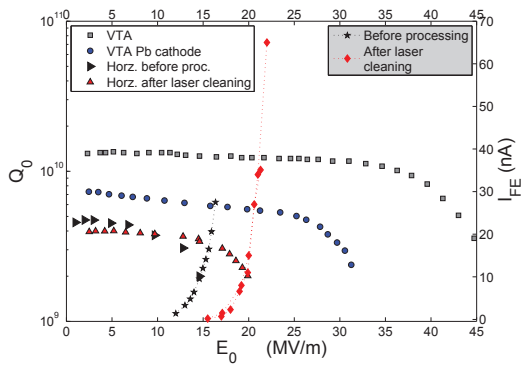

Figure 3: Measured unloaded quality factor Q_0 of cavity 0.1 versus on axis peak electric field after cavity assembly and treatment in the vertical test stand (grey squares) at JLab, after deposition of the cathode (blue circles), the first horizontal test after installation and beam line assembly at HZB (black triangles) and after laser cleaning of the lead cathode(red triangles).

ISBN 978-3-95450-143-4

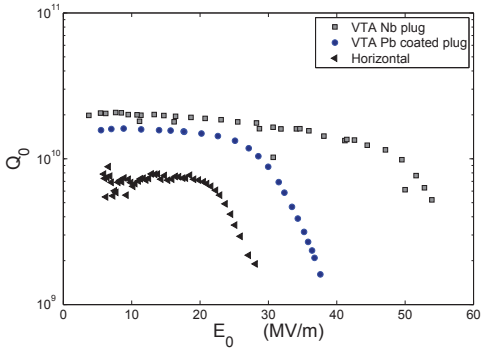

Figure 4: Q_0 vs. E_0 of cavity 0.2 in the vertical test stand with the uncoated Nb plug installed (grey squares), after installation of the lead coated plug (blue circles) and finally calorimetrically measured Q_0 at the horizontal test facility at HZB including the diagnostic beamline.

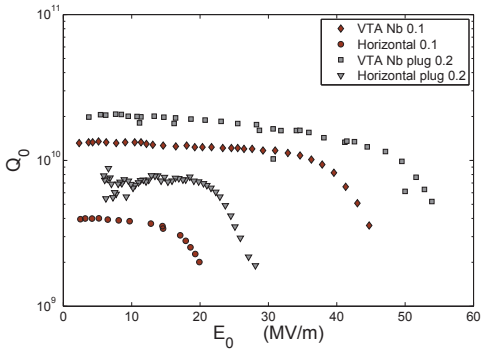

Figure 5: A comparison of the vertical and horizontal test results of $Q_0(E_0)$ for cavities 0.1 and 0.2.

suming same surface resistance is only $3.6 \cdot 10^{-6}\%$ and for the whole plug about $2 \cdot 10^{-4}\%$. Finally, after transport to Berlin and installation in HoBiCaT, the measured quality factor was again decreased by a factor of two for cavity 0.2, for cavity 0.1 the Q_0s were in general a factor of two lower than for the second cavity and it further features a much earlier onset of field emission at 12 MV/m in the horizontal tests. After laser cleaning of the cathode it improved to 18 MV/m [2, 13]. The maximum operating fields were thus limited to 20 MV/m for cavity 0.1 due to a strong contribution by dark current, whereas cavity 0.2 was able to operate up to 27 MV/m. Cavity 0.1 was installed in HoBiCaT with two magnetic shields whereas cavity 0.2 was not equipped with a second shielding. Cavity 0.2 had a residual resistance of 35 nΩ in the horizontal tests. This cannot be explained by the missing shielding, as the remnant magnetic field in HoBiCaT is about 1-2 μT.

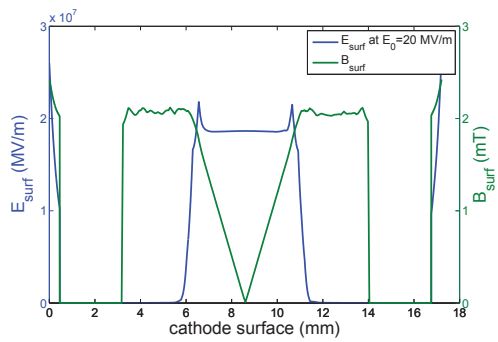

Figure 6: Electric and magnetic surface field distribution of the TM_{010}-π mode on the plug surface. These calculations were done using CST MWS [12] in order to understand possible loss mechanisms observed at the plug location.

Findings with the plug design First RF tests in HoBiCaT showed a rather low achievable field and strong multipacting of the plug design at field levels of 3 and 8 MV/m. This was correlated with an increase of the cavity and beam line vacuum to $1 \cdot 10^{-7}$ [14]. Most likely this was a λ-leak between the superfluid helium bath and inner cavity caused by the indium seal of the plug, even though special care was taken for a proper installation. Nevertheless, by RF processing the peak fields were increased to 27 MV/m, the multipacting barriers can even be passed running with an LLRF system, instead of the phase-locked loop used for the quality factor measurements. The processing came along with a decrease of the observed radiation level 1.5 m downstream the cryostat by three orders of magnitude. The first notable dark current was seen at 25 MV/m. The cavity quenched instantaneously at 28 MV/m. At 25 MV/m it took about one hour of continuous operation for the quench to manifest itself. As depicted in Figure 7 a slow heating and increase in helium consumption comes along with field levels beyond 24 MV/m. The increase in temperature was measured in the liquid at the back wall of the rather thick Nb plug. We suspect to have a bad thermal contact between the cooled cavity back wall and the plug system leading to

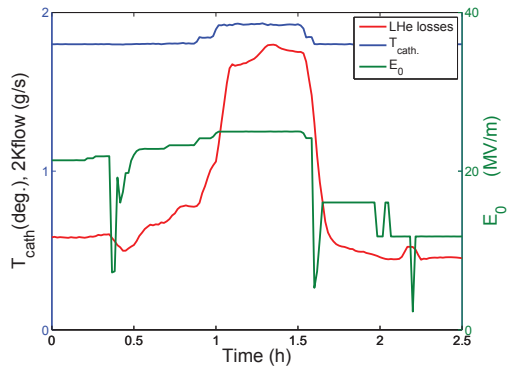

Figure 7: Quench event of cavity 0.2 close to the instantaneous quench field level at 28 MV/m. It was operated at E_0=25 MV/m (green line), a strong increase of the dissipated power into the superfluid helium was observed (red line, 2 K flow) and an increase of the temperature measured on the solid back wall of the Nb plug was observed.

a warming and finally quench at the cathode and even indium seal location.

QE and dark current The measured field emitted dark current originated mainly from the cathode area as was demonstrated with tracking calculations by V. Volkov [2]. Figure 8 shows dark current of both cavities at different field levels focussed by the SC solenoid on the first view screen. For the plug design the dark current seems to be a mapping of the plug's gap area, comparable with the high electric field distribution shown before in Figure 6.

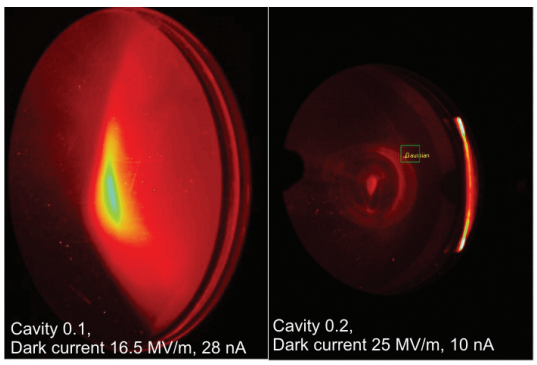

Figure 8: Comparison of dark current for both cavities measured at the first screen at different field levels using the solenoid to focus the beam. The field emission onset of cavity 0.2 was significantly higher than for cavity 0.1, especially after additional RF processing.

It is mainly caused by irregularities in the morphology and tip on tip like substructures of the lead coating. Especially for cavity 0.1 small droplets were observed and areas of dark current were identified to have a rather small QE and a strong fluorescence in the visible regime when illuminated by the cathode laser [13, 15]. The plug cathode featured a smoother and also more isotropic surface regarding the QE distribution and therefore much less dark current. The same appears for the fluorescence maps taken without field illuminating the cathode with the drive laser and taking pictures with a CCD in the visible regime.

With cavity 0.1 at areas of very low QE and strong fluorescence strong field emitters exploded with currents at least ten times higher than the wanted beam when illuminated with the cathode laser at specific RF field level [2]. After this procedure these field emitters seemed to be removed, the fluorescence level was reduced. This shows, that for contaminated cathodes even with the cathode laser some cleaning of the cathodes is possible. But for an overall increase of the QE a laser cleaning is mandatory.

Figure 9 shows the QE obtained with the lead cathode of cavity 0.1 before and after laser cleaning with a KrF excimer laser at 248 nm compared to values achieved with samples [16]. The values are below the best witness samples but exceed the QE of cleaned Nb by a factor of five. Unfortunately there was no measurement time to perform laser cleaning with the plug cavity, but it achieved similar

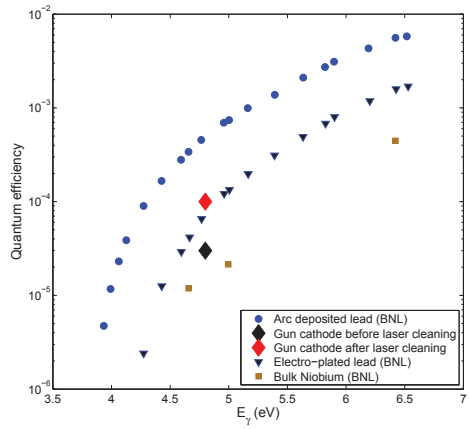

Figure 9: Comparison of measured quantum efficiency (QE) versus laser pulse energy at BNL [7] of electro-plated, arc-deposited lead and bulk Niobium samples with the QE obtained for the arc-deposited lead cathode of cavity 0.1 before and after laser cleaning.

QE as the uncleaned back wall cathode, but with a much more uniform distribution. Summing up, lead cathodes allow only small beam currents, but they are very robust against contaminations and processing of field emitters and can be brought back to full performance by laser cleaning.

Operational Experience, Field Stability

Both cavities were operated with a modified version of Cornell's LLRF system [17]. Cavity 0.2 is even equipped with a Saclay tuner system, whereas with cavity 0.1 the master clock for LLRF and laser system referenced to a lowpass filtered phase locked loop following cavity drifts. Figure 10 depicts the piezo modulation to RF detuning

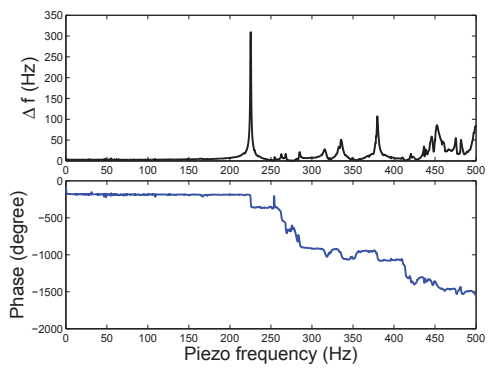

Figure 10: Measured piezo to RF detuning transfer function of the piezo stacks installed in the adapted Saclay I style tuner. The first mechanical eigenmode appears at 248 Hz

transfer function of the Saclay tuner installed with cavity 0.2. The response is very flat until the first mechanical eigenmode appearing at 248 Hz, beyond the loaded Q

ISBN 978-3-95450-143-4

bandwidth of the cavity. The measured detuning spectra (Figure 11) mainly feature external vibrations acting on the cavity. Using a heater to simulate RF losses within the liquid helium it was shown, that the spectral lines appearing for higher losses are correlated with activity in the helium bath (LHe). These spectral lines below 100 Hz appear to increase with the localized losses produced by the heater. This increase of dynamics of the LHe bath at field levels

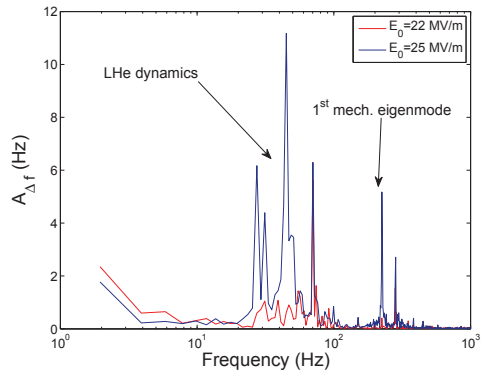

Figure 11: Measured microphonics detuning spectrum at two different field levels. At about 25 MV/m strong activity in the helium bath takes place and an increase of the excited first mechanical eigenmode was observed.

near the quench level, where a warming of the cathode region leads to a localized increase of the heat deposited in the bath, comes along with an increase of the mechanical eigenmode detuning contribution. More measurements about heat transport within the helium bath, LHe heat transport capacity and measured microphonics are planned for the future.

Table 2 gives an overview of the field stability and measured detuning levels for different scenarios of both cavities. Beam energy modulation experiments using the piezo tuner have shown, that the contribution of the phase and amplitude stability compared to laser time jitter and laser pulse length to the beam's energy jitter is negligible.

Table 2: Cavity field stabilities and detuning measured at different field levels for both cavities

Q_L	E_0 (MV/m)	σ_f (Hz)	σ_Φ (deg)	σ_A/A
Cavity 0.1				
$1.4 \cdot 10^7$	12.0	5.02	0.02	$1.5 \cdot 10^{-4}$
$6.6 \cdot 10^6$	20.0	7.0	0.017	$1.2 \cdot 10^{-4}$
Cavity 0.2				
$6.6 \cdot 10^6$	22.0	5.6	0.026	$1.1 \cdot 10^{-4}$
$6.6 \cdot 10^6$	25.0	13.8	0.039	$1.6 \cdot 10^{-4}$

Beam Parameters and Quantum Efficiency Measurements

Besides studying the RF parameters and achievable surface resistance and field limits, the main goal was to understand the beam dynamics within the injector cavity and to measure the beam's phase space to extract the emittance. Table 3 gives an overview of the obtained beam and field parameters achieved with the two versions of the PbNb hybrid cavity. The same UV 258 nm cathode laser was used for both measurement runs, operating at 8 kHz. For all emittance measurements the space charge contribution was negligibly low with charges below 1pC and short pulses to omit RF curvature contributions. To determine the normalized emittance both the slit mask and solenoid scan methods were applied. More details about the beam measurements can be found in [1, 18, 19]. In summary one could

Table 3: This table summarizes typical beam parameters and cavity settings for both PbNb hybrid cavities illuminated with 258 nm cathode laser at 8 kHz repetition rate at the given maximum on axis fields.

Parameter	**0.1**	**0.2**
Cathode type	Pb back wall	Pb plug
Cathode $QE_{\max}$	$1 \cdot 10^{-4}$	$1 \cdot 10^{-5}$
E_0max.	20 MV/m	27 MV/m
E_{launch}	5 MV/m	7 MV/m
E_{kin} at max. E_0	1.8 MeV	2.5 MeV
Bunch charge	6 pC	187 fC
Emission time	2-4 ps	2.5-3 ps
Average current	50 nA	1.5 nA
Normalized emittance/mm	5.4	1.9
laser spot size	mm mrad	mm mrad

state, that due to the improved cathode deposition technique, as already discussed with the QE and dark current, a much more smoother surface with less protrusions and droplets was achieved. This resulted in a lower dark current level, higher achievable fields and finally a lower beam emittance, as the cathode morphology directly contributes to the thermal emittance as discussed in [18].

Another hint for the cathode surface structure contributing to the overall emittance is given by the transverse phase space measurement shown in Figure 12. This measurement was done at E_0=10 MV/m and 15 deg. emission phase, as at that time a failure of the IOT limited the available forward power. For large laser spot sizes, as given here by 0.66 mm RMS, a substructure of the transverse divergence across the vertical bunch coordinate hints at different emission points with different thermal emittance contributions. Figure 13 gives an overview about the phase dependance of the kinetic beam energy for different field levels. For higher fields, though not visible in the plot, a maximum appears at low phases of about 15 deg.

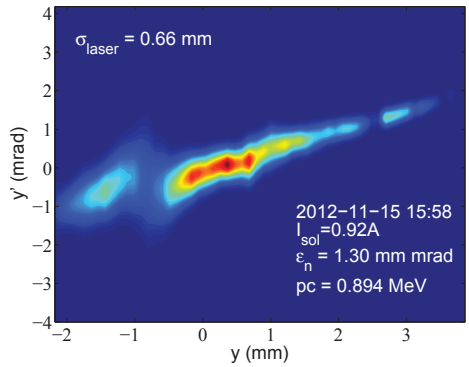

Figure 12: Reconstruction of vertical phase space at E_0=10.0 MV/m for cavity 0.2.

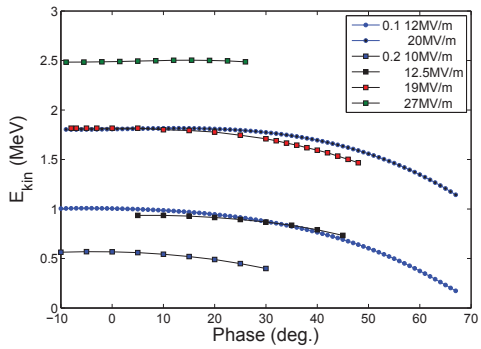

Figure 13: Measured kinetic beam energies E_{kin} at different field levels for both cavities versus emission phase with respect to the RF field.

AN INJECTOR FOR B*ERL*inPro

Experience gained with the measurements of the cavity 0.1 folded with the requirements of the B*ERL*inPro project resulted in the design of the next injector cavity towards the full power 100 mA version. The first step, called cavity 1.1, should demonstrate the beam dynamics requirements for the ERL with respect to emittance, energy spread, jitter requirements, dark current studies and peak brightness at the full charge of 77 pC and currents up to 4 mA. Thus, a normal conducting semiconductor cathode has to be implemented.

The final cavity geometry was an outcome of a combined RF and tracking simulation to optimize parameters as e.g. skew back wall and path length of the half cell. This process ended up in a $1.4{\cdot}\lambda/2$ cell design, to mainly achieve a higher launch phase compared to cavity 0.1 to have an effective ratio of maximum surface field and field seen by the beam.

RF Design

Thus a whole new RF design [20] was created accounting for:

- A high launch phase for the maximum energy gain under the given forward power constraint. This should guarantee a high emission field to compensate for space charge driven beam expansion, as the fraction of maximum on-axis field to emission field level is minimized. The longitudinal on-axis field for different cathode positions is presented in Figure 14.
- Further, to account for the avoidance of dark current, the maximum on axis field level is not located on the cathode surface (which has a low work function) itself, but close after. This is achieved by a skew back wall and the curvature of the cathode insert opening. This also features transverse field components for beam focussing.
- Finally by fine tuning the design the electric peak surface field was moved from the cathode opening to the inner iris towards the back wall. This is a less probable origin for field emitted particles to leave the structure contributing to dark current transported through the accelerator.

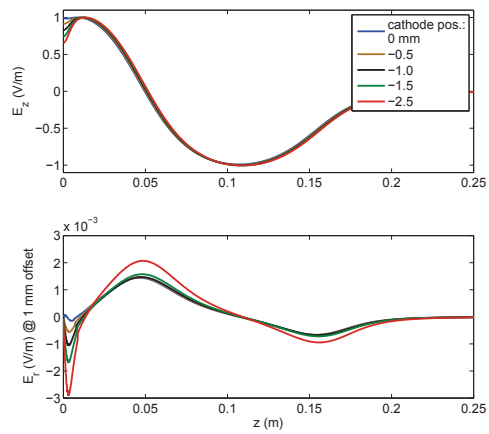

Figure 14: Longitudinal electric field component at r=0 mm and radial electric field at r=1 mm versus z for different cathode positions.

Table 4 summarizes the cavity RF properties calculated by Superfish [21] and CST MWS.

Ancillary Equipment

A sketch of the cavity and its ancillary components is given in Figure 15. It shows the 1.4 cavity cell with the cathode opening in the back wall followed by the HZDR style insert system of choke cell and Petrov filter. The beam tube is enlarged such to allow for propagation of the lowest dipole mode and still coupling of two CW-modified TTF-III coupler [22] delivering up to 10 kW each. The coupling is optimized for low kick and a beam current of 4mA. Downstream the beam tube will be the superconducting solenoid followed by a beam tube HOM absorber. The cavity will be equipped with a blade tuner system similar to the Cornell version including four piezos for fine tuning.

ISBN 978-3-95450-143-4

Table 4: Cavity figures of merit for the TM_{010}-π mode of injector cavity 1.1 at E_0= 30 MV/m and cathode retracted from 0-2.5 mm. Note, that Q_{ext} is optimized for 4 mA beam current.

Parameter	Cavity 1.1
$R/Q(\Omega)$	150-149.5
E_{peak}/E_0	1.5-1.45
$E_{cathode}/E_0$	1-0.58
B_{peak}/E_{peak} (mT/(MV/m))	2.2
$\Phi_{launch}(E_{kin,max})$ (deg.)	60-50
E_{launch} (MV/m)	26-13.3
E_{kin} (MeV)	2.6
k_{cc} (%)	1.6
Q_{ext}	$3.6 \cdot 10^6$
$f_{1/2}$(Hz)	185
$P_{forward}$ (kW)	8.4
$\Delta f/\Delta P_{LHe}$ (Hz/mbar)	10 (expected)
I_{avg} (mA)	4
Q_b (pC)	77

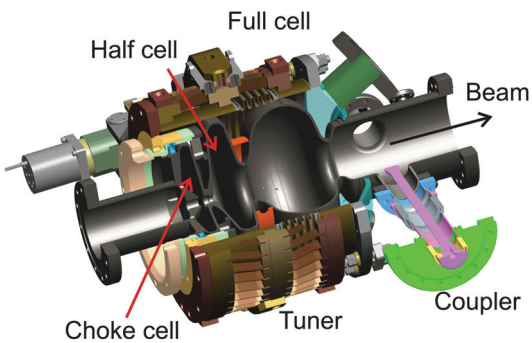

Figure 15: Drawing of the SRF photo-injector cavity with the cavity, beam tube, choke cell and cathode insert in silver grey. Also shown are ancillary components such as the helium vessel, blade tuner, stiffening ring and CW-modified TTF-III coupler.

Combined electro-magnetic-mechanical calculations by E. Zaplatin [23] were performed in order to find a stiffening ring position and material thickness for minimum detuning to pressure sensitivity of the cavity $\Delta f/\Delta P_{LHe}$. The expected tuning sensitivity will be 1.6 MHz/mm and $\Delta f/\Delta P_{LHe}$ ≈10 Hz/mbar. Tuning the structure by 300 kHz will result in a maximum field flatness change of 3%, below tolerances for beam dynamics considerations.

At the moment, this cavity is being manufactured at JLab and will see its first vertical RF test presumably Fall of this year. A first impression of the half cell manufacturing can be obtained from the picture in Figure 16 showing three of the four half cell sections and the beam tube stacked for mechanical inspection.

Figure 16: Cavity 1.1 in production at JLab. Here the cavity is only stacked and the first half of the $0.4{\cdot}\lambda/2$ cell is missing.

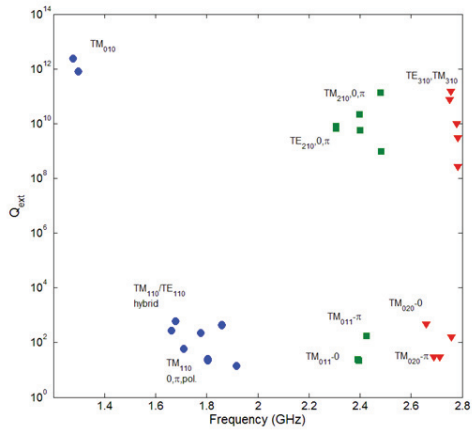

Figure 17: Calculated Q_{ext} for modes up to 3 GHz for a port at the HOM absorber location.

HOM Studies

HOM calculations of the current design have shown, that higher order monopole modes and dipole modes are leaving the structure propagating to the beam tube absorber (see Figure 17). But some quadrupole modes seem to be trapped within the half cell. Further it has to be taken into account, that the R/Q depend on the evolution of β within the cavity cells and thus on the maximum on axis field level. Calculations have shown [20], that for monopole π modes $R/Q_{\parallel}$ increases with E_0 and decreases for the zero mode. For dipole modes $R/Q_{\perp}$ behaves in the opposite manner.

OUTLOOK: CAVITY 2.1

The high power cavity version will be equipped with two KEK-style couplers which were modified in design using a golf tee shaped tip form for improved coupling and reduced coupler kick. For this cavity version it has to be understood whether the trapped quadrupole and sextupole modes play

any role in unwanted beam cavity interaction and how to change cell-to-cell coupling and the exit iris to allow even those modes to escape. Further work has already started to improve and simplify the choke cell design as well as the cooling of the cathode plug at the expected RF losses and laser power.

ACKNOWLEDGEMENTS

The authors would like to thank the large group of people who allowed the realization of these results with their contributed work. Especially we would like to thank the co-workers at DESY, JLAB and NCBJ who invested their time and effort to construct and manufacture the two NbPb cavities, as well as the group at HZB helping in the operation of HoBiCaT, designing ancillary components and mounting the experimental set up. For the current cavity production we would like to acknowledge the technical personnel at JLab. For many fruitful discussion about the cathode systems and for providing the drawings our partners at Helmholtz Zentrum Dresden, especially J. Teichert, P. Murcek and A. Arnold are thanked.

REFERENCES

[1] T. Kamps et al., IPAC'11, San-Sebástian, September 2011, THPC109, p. 3143, http://www.JACoW.org.

[2] A. Neumann et al., IPAC'11, San-Sebástian, September 2011, MOODA03, p. 41, http://www.JACoW.org.

[3] J. Knobloch et al., ICFA Beam Dynamics Newsletters, No.58, p. 118, August 2012, http://www-bd.fnal.gov/icfabd/Newsletter58.pdf.

[4] J. Sekutowicz, A. Muhs, P. Kneisel, R. Nietubyc, Proc. of the 23rd PAC (2009), Vancouver, Canada, http://www.JACoW.org.

[5] A. Neumann et al., LINAC'12, Tel Aviv, September 2012, THPB066, p. 993, http://www.JACoW.org.

[6] T. Kamps et al., LINAC'12, Tel Aviv, September 2012, THPB069, p. 993, http://www.JACoW.org.

[7] A. Arnold et al., Nuclear Instruments and Methods in Physics Research Section A, Volume 593, Issues 12, 1 August 2008, Pages 57-62, DOI 10.1016/j.nima.2008.04.035.

[8] S. Noguchi et al., IPAC'10, Kyoto, 2010, WEPEC024, p. 2944, http://www.JACoW.org.

[9] R. Nietubyć et al., IPAC'10, Tsukuba, May 2010, THPEC020, p. 4086, http://www.JACoW.org.

[10] P. Kneisel *et al.*, Proc. of the 24th PAC (2011), New York, USA, p. 1047, http://www.JACoW.org.

[11] A. Neumann *et al.*, Proc. of the 25th LINAC (2010), Tsukuba, Japan, http://www.JACoW.org.

[12] Computer Simulation Technology AG, Microwave Studio®, 64289 Darmstadt, Germany http://www.cst.com.

[13] R. Barday et al., IPAC'13, Shanghai, May 2013, MOPFI001, p. 279, http://www.JACoW.org.

[14] A. Burrill et al., IPAC'13, Shanghai, May 2013, WEPWO002, p. 2313, http://www.JACoW.org

[15] R. Barday et al., submitted to PRST-AB:*Characterization of a Superconducting Pb Photocathode in an SRF Photoinjector Cavity*, August 2013.

[16] J. Smedley *et al.*, *Lead photocathodes*, PRST-AB, Volume 11, No. **1**, 2008, DOI: 10.1103/PhysRevSTAB.11.013502.

[17] M. Liepe *et al.*, Proc. of the 21st PAC (2005), Knoxville, USA, http://www.JACoW.org.

[18] J. Voelker et al., IPAC'12, New Orleans, May 2012, TUPPD051, p. 1518, http://www.JACoW.org.

[19] M. Schmeisser et al., IPAC'13, Shanghai, May 2013, MOPFI002, p. 282, http://www.JACoW.org.

[20] A. Neumann et al., IPAC'13, Shanghai, May 2013, MOPFI003, p. 285, http://www.JACoW.org.

[21] K. Halbach and R.F. Holsinger, *SUPERFISH - a computer program for evaluation of RF cavities with cylindrical symmetry*, Part. Acc., 7:213222, 1976.

[22] O. Kugeler et al., SRF'09, Berlin, Germany, September 2009, THPPO046, p. 683, http://www.JACoW.org.

[23] E. Zaplatin et al., IPAC'13, Shanghai, May 2013, WEPWO009, p. 2328, http://www.JACoW.org.

ISBN 978-3-95450-143-4